World Automation Congress @ 2010 TSI Press.

Vision-Guided Individual Modeling of Bendable Cables for Their Insertion

(Yuuki Kataoka and Shinichi Hirai)
Department of Robotics, Ritsumeikan University,
Kusatsu, Shiga 525-8577, Japan

Abstract

This paper focuses on modeling of bendable cables based on their visual measurement of static and dynamic deformation. Cable insertion is one of basic operations in electric and automotive industries. Automatic insertion is desired but the insertion is still done by humans. The barrier against the automatic insertion of bendable cables is the variance of their deformed shapes. Here we will propose vision-guided *individual modeling* to cope such variance.

First, we show a model of bendable cables with nonlinear flexural elasticity. Second, we describe the identification of model parameters for individual cables based on their visually measured deformation. Experimental verification demonstrates the proposed approach.
Keywords vision, deformation, modeling.

1 Introduction

This paper presents a modeling of individual cables based on their visual measurement of static and dynamic deformation. Cable insertion is one of basic operations; this operation often appears in electric and automotive industries. This operation depends on human work up to now though automatic insertion is desired for the past decades. The barrier against the automatic insertion of bendable cables is the variance of their deformed shapes. Individual cables exhibit different deformation, even though their natural shapes are identical. This suggests that motion of an assembly robot must change according to individual cables. Manipulation of deformable objects has been studies in the past decade [1, 2, 3]. Insertion of flexible wires has been studies [4, 5, 6, 7] but the variance among wires is out of focus.

One approach to change the motion of an assembly robot is *visual servoing*, where visual images are fedback to the robot synchronously to the robot motion. This approach can cope with any deformation that may happen in actual operation. Unfortunately, capturing successive images, transmitting them to a image processor, and image processing synchronous to robot motion control require special hardwares, which results in high cost and low applicability. Thus, alternative approach is needed.

Individual cables exhibit different deformation, implying that a set of physical parameters of each cable differs from one another. But, the set of parameters appears to be time-invariant, since deformations of one cable coincide one another. Thus, once the set of parameters of each cable is identified, we can simulation the deformation of the cable so that the insertion will be successful. This paper apply this approach, which is referred to as *individual modeling*. Modeling of deformable objects has been studied extensively [8, 9, 10]. Modeling of linear objects has been proposed [11, 12, 13, 14, 15]. Unfortunately, identification of linear object models has not studied well.

In Section 2, we will show the insertion of bendable cables in the vertical plane. Section 3 presents the modeling of individual cables based on their static and dynamic deformation. Section 5 shows experimental results on individual modeling of cables as well as the guidance of cables. Section 6 concludes this paper.

2 Insertion of Bendable Cables

Figure 1 illustrates the operation to be tackled in this paper. Operation is to guide the top of a bendable cable to the predetermined destination area, which represents a hole in which the cable inserted. We focus on two-dimensional deformation of a cable. An assembly robot, which works in the vertical plane, grips a bendable cable at one point on the cable. The gripping point is apart from the top so that the cable can be inserted into the hole.

Figure 2 demonstrates static deformation of cables. We used flat cables of thickness 0.1 mm, width 16.0 mm, and line density of 7.4 g/m. A robot grasps a flat cable at the point 100 mm apart from its top. Figure 2-(a) shows a superimposed image that shows the deformation of eight cables. As shown in

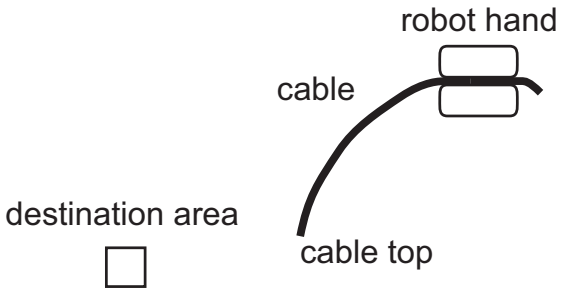

Figure 1: Operation to guide the table top to destination area

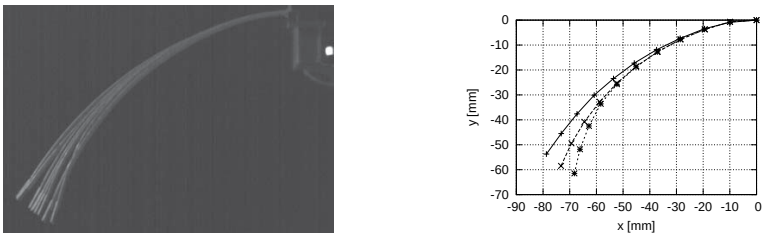

(a) measured deformation of eight cables (b) deformation of three cables

Figure 2: Different deformation of cables with same geometry

the figure, the static shapes of eight deformed cables differ from one another. The difference at the top reached to 13.04 mm at its maximum. We applied a sequence of image processing algorithms to extract the deformed shape of a cable. We divided the total length of a cable into 10 regions, implying that the extracted shape consists of 11 points. Figure 2-(b) shows the extracted shape of three deformed shapes out of measured deformations given in Figure 2-(a).

Figure 3 demonstrates dynamic deformation of a cable. Moving the gripping point 50 mm downward by an assembly robot yields the vibration of the top of a cable. Figures 3-(a) and (b) describe the vertical and horizontal trajectories of the cable top and the gripping point. As shown in the figures, the cable top trajectory differs from the gripping point trajectory, implying that the cable deforms dynamically during the operation. Consequently, we have to cope with the variance of cable deformation as well as dynamic deformation of cables to perform the insertion of bendable cables.

3 Model of Bendable Cables

We focus on cable deformation in two-dimensional vertical plane. Assuming that the cable thickness is negligible, we find that the deformed shape is described by a curve in the vertical plane. Assume that

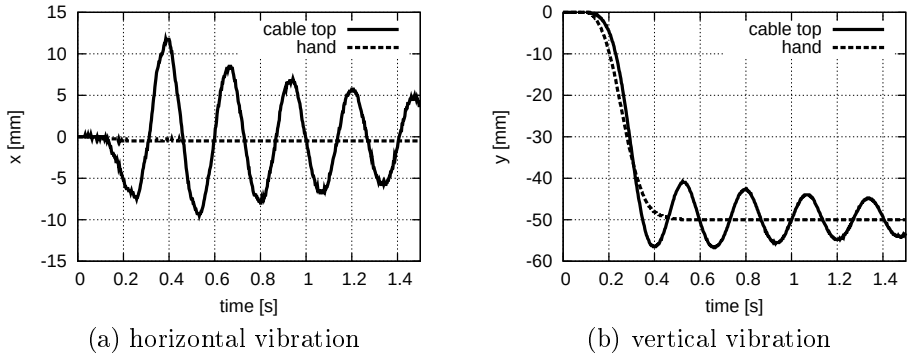

(a) horizontal vibration (b) vertical vibration

Figure 3: Dynamic deformation of cable

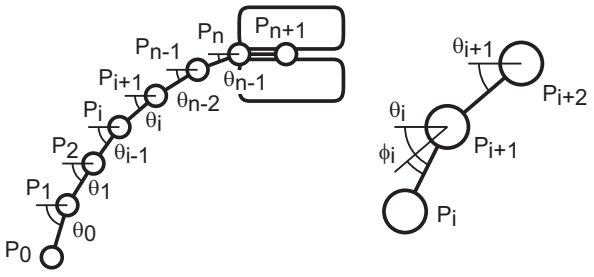

(a) angle from horizon (b) bending angle

Figure 4: Cable model

a robot grasps a cable and grasping region is given by horizontal planes. The deformed shape is given by the free side of the cable. Let us approximate the deformed shape of a cable by a sequence of n line segments, as illustrated in Figure 4-(a). Let P_0 be the top nodal point of the cable and P_n be its base point. The deformed shape of a cable is then described by $(n+1)$ nodal points. Dynamic deformation of a cable is determined by these nodal points $_0$ through P_n. Additionally, let us introduce nodal point P_{n+1} to describe the region of a cable gripped by a robot. Note that the position of P_n and P_{n+1} is determined by the motion of the robot.

We apply particle-based modeling; mass of a cable is distributed to nodal points. Let us equally distribute the mass of a cable into n nodal points; $_0$ through P_{n-1}. Let m be the mass of these nodal points. Let θ_i $(i = 0, 1, \cdots, n-1)$ be the angle from the horizon of line segment $\mathrm{P}_{i+1}\mathrm{P}_i$. Since grasping region is a horizontal plane, let $\theta_n = 0$. Then, as illustrated in Figure 4-(b), bend angle of a cable at P_{i+1} is given by ϕ_i, which is defined as

$$\phi_i = \theta_i - \theta_{i+1}, \quad (i = 0, 1, \cdots, n-1). \tag{1}$$

Let l be the length of line segments. Let $\boldsymbol{x}_i = [x_i,\ y_i]^{\mathrm{T}}$ be the position vector of P_i, which is described by

$$\boldsymbol{x}_i = \boldsymbol{x}_n - l \sum_{j=i}^{n-1} \begin{bmatrix} \cos\theta_j \\ \sin\theta_j \end{bmatrix}, \tag{2}$$

where $\boldsymbol{x}_n$ is determined by the motion of a robot.

Let K_i be the coefficient of flexural rigidity corresponding to angle ϕ_i. Flexural potential energy of the cable is then formulated as

$$U_{\mathrm{flex}} = \sum_{i=0}^{n-1} \frac{1}{2} K_i \phi_i^2. \tag{3}$$

Gravitational potential energy is simply formulated as

$$U_{\mathrm{grav}} = \sum_{i=0}^{n-1} mgy_i. \tag{4}$$

Total potential energy is given by the sum of the above two energies:

$$U = U_{\mathrm{flex}} + U_{\mathrm{grav}}. \tag{5}$$

According to the variational principle statics, the above potential energy reaches to its minimum at the stable deformation of a cable, implying that the partial derivatives of the potential energy with respect to ϕ_1 to ϕ_n vanish:

$$\frac{\partial U}{\partial \phi_i} = 0, \quad (i = 0, 1, \cdots, n-1). \tag{6}$$

Computing the above partial derivatives, we have

$$K_i\phi_i - mgl \sum_{k=i}^{n} (n-k)\cos\theta_k = 0, \quad (i = 0, 1, \cdots, n-1). \tag{7}$$

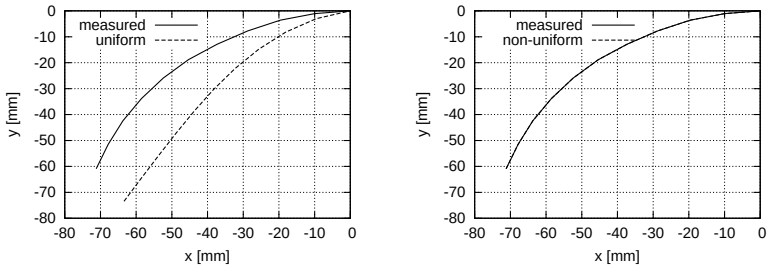

(a) uniform model (b) non-uniform model

Figure 5: Comparison between uniform and non-uniform models

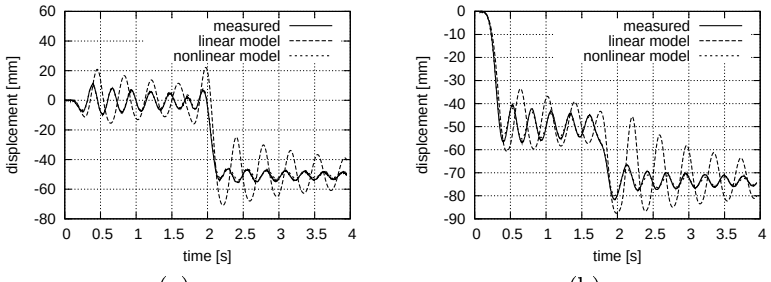

(a) x (b) y

Figure 6: Comparison between linear and nonlinear models

Note that the first term $K_i\phi_i$ denotes linear elastic torque caused by cable bending. We can replace this term by any nonlinear term. In this paper, we will apply the following term:

$$\tau_i = K_i\phi_i^N, \tag{8}$$

where N be the exponent Here we assume the bending stiffness is not uniform. In addition, we introduce exponent n to describe nonlinear nature of the cable bending.

In the formulation of dynamic deformation, we will introduce viscous term, resulting in

$$\tau_i = K_i\phi_i^N + C\dot{\phi}_i, \tag{9}$$

where C be the coefficient of bending viscosity. Torque around P_i is equivalently converted into forces at P_i and its two neighboring nodal points, P_{i-1} and P_{i+1}. In addition, we will introduce virtual an extensional Voigt model between neighboring nodal points so that the length of a line segment remains l. Selecting a large value for the spring coefficient of the virtual Voigt model, the length of a line segment remains almost equal to l. Solving the dynamic equations of motion with respect to $\boldsymbol{x}_0$ through $\boldsymbol{x}_{n-1}$ under given $\boldsymbol{x}_n$, we can compute the deformation of a cable.

4 Individual Modeling of Cables

This section focuses on the individual modeling of bendable cables. A stable deformed shape satisfies the following equations:

$$K_i\phi_i^N = mgl\sum_{k=i}^{n}(n-k)\cos\phi_k, \quad (i = 0, 1, \cdots, n-1). \tag{10}$$

Static shape of a cable determines ϕ_i as well as θ_i. Given a value to exponent N, we can compute flexural coefficients K_0 through K_{n-1}.

Exponent N and viscous coefficient C affect the dynamic deformation of a cable. Figure 7 demonstrates the contribution of model parameters to cable top vibration. Frequency of vibration depends on exponent N, as shown in Figure 7-(a). Viscous coefficient C mainly affects the damping ratio of the vibration, as

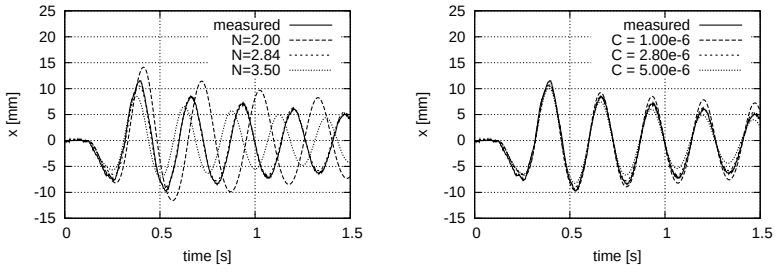

(a) exponent N (b) viscous coefficient C

Figure 7: Contribution of parameters to cable top vibration

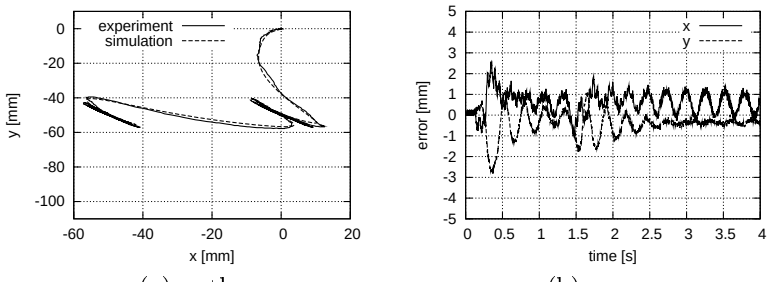

(a) path (b) error

Figure 8: Cable top motion with vertical displacement 0 mm

shown in Figure 7-(b). Once K_0 through K_{n-1} are determined, we can select appropriate values of N and C by comparing the measured dynamic deformation with simulation result. Iterating the computation of K_0 through K_{n-1} using static deformation and the computation of N and C using dynamic deformation, we finally identify K_0 through K_{n-1}, N, and C.

5 Experimental Results

We have used cables used in Section 2. A robot grasps a flat cable at the point 100 mm apart from its top. The robot hand then moves from its initial position 50 mm downward and keeps its position for 1000 ms. Assume that parameters of a cable are identified during this period. Then, the robot hand moves downward by 0 mm, 10 mm, 20 mm, 30 mm, or 40 mm, then moves 50 mm leftward.

Figure 8 shows the motion of the cable top when the robot hand moves downward by 0 mm, then moves 50 mm leftward. Figure 8-(a) shows experimental and simulated results. Figure 8-(b) denotes the error between the two results. Figure 9 shows the motion of the cable top when the robot hand moves downward by 10 mm, then moves 50 mm leftward. Figure 10 shows the motion of the cable top when the robot hand moves downward by 20 mm, then moves 50 mm leftward. Figure 11 shows the motion of

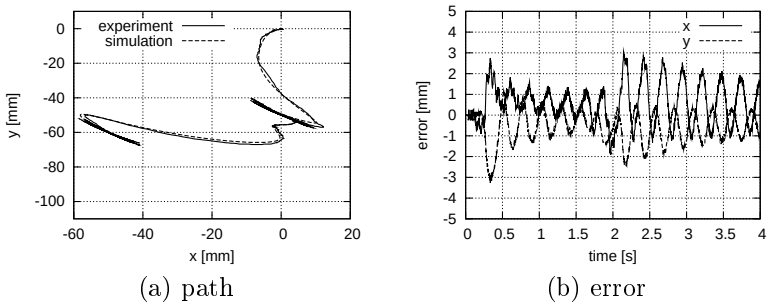

(a) path (b) error

Figure 9: Cable top motion with vertical displacement 10 mm

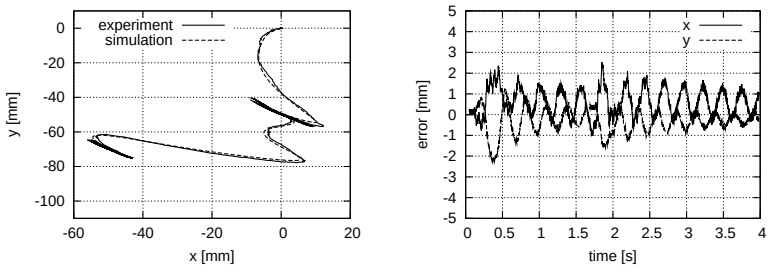

(a) path (b) error

Figure 10: Cable top motion with vertical displacement 20 mm

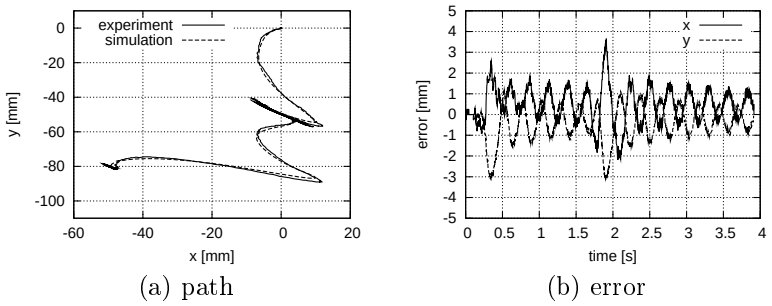

(a) path (b) error

Figure 11: Cable top motion with vertical displacement 30 mm

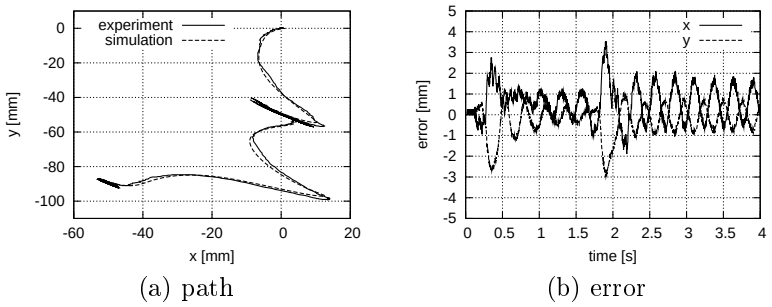

(a) path (b) error

Figure 12: Cable top motion with vertical displacement 40 mm

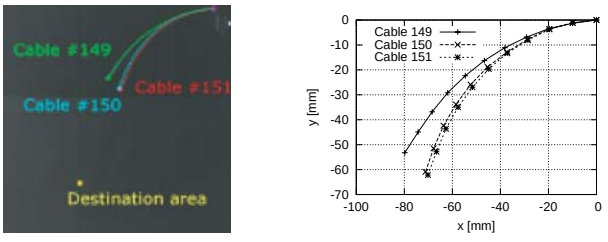

(a) measured deformation (b) extracted deformation

Figure 13: Three cables used in experiment

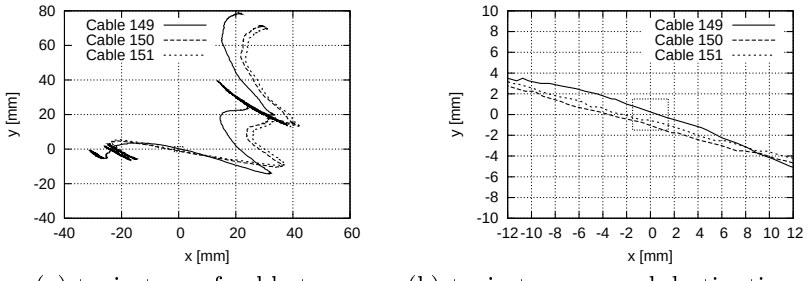

(a) trajectory of cable top (b) trajectory around destination area

Figure 14: Trajectory of cable top for selected operation

the cable top when the robot hand moves downward by 30 mm, then moves 50 mm leftward. Figure 12 shows the motion of the cable top when the robot hand moves downward by 40 mm, then moves 50 mm leftward. As shown in the figures, simulation results almost agree with experimental results, implying that we can estimate the dynamic deformation of a cable through simulation once parameters of the cable are identified.

Let us verify if the cable top of cables can be guided to the destination area. We used three cables shown in Figure 13. As shown in Figure 13-(a), the cables exhibit different static shapes. Figure 13-(b) describes the extracted nodal points of each cable, which are used in identification. Figure 14 shows the trajectories of the cable top of the three cables. As shown in Figure 14-(a), the three trajectories differ one another but all trajectories pass the destination area, as shown in Figure 14-(b). In this case, one of downward distance was selected among 21 distances between 0 mm and 40 mm with interval of 2 mm, so that the cable top passes the destination area. Figure 15 denotes both cable top motion and robot hand motion. As shown in the figure, robot downward motion depends on cables.

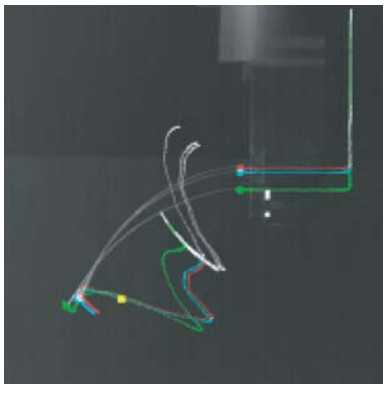

Figure 15: Cable top motion and robot hand motion

6 Conclusion

We have proposed vision-guided modeling of individual cables. We used static and dynamic deformation of a cable to build an individual model. We showed that the simulated deformation almost agreed with actual deformation and that the cable top passed destination area once individual model was built.

Individual modeling requires many dynamic simulations, which consume much time. We have to speed up the simulation for reduce the time for individual modeling. We need to introduce visual feedback to reduce the current error.

Acknowledgement

This research was supported by Canon Inc.

References

[1] Taylor, P. M. *et al.*, *Sensory Robotics for the Handling of Limp Materials*, Springer–Verlag, 1990.

[2] Henrich, D. and Wörn, H. eds., *Robot Manipulation of Deformable Objects*, Springer–Verlag, Advanced Manufacturing Series, 2000.

[3] Shibata, M., Ota, T., and Hirai, S., *Wiping Motion for Deformable Object Handling*, Proc. IEEE Int. Conf. on Robotics and Automation, pp.134–139, Kobe, May 12-17, 2009.

[4] Zheng, Y. F., Pei, R., and Chen, C., *Strategies for Automatic Assembly of Deformable Objects*, Proc. IEEE Int. Conf. on Robotics and Automation, pp.2598–2603, 1991.

[5] Chen, M. Z. and Zheng, Y. F., *Vibration-Free Handling of Deformable Beams by Robot End-Effectors*, Journal of Robotic Systems, Vol. 12, No. 5, pp.331–347, 1995.

[6] Nakagaki, H., Kitagaki, K., Ogasawara, T., and Tsukune, H., *Study of Deformation and Insertion Tasks of a Flexible Wire*, Proc. IEEE Int. Conf. Robotics and Automation, pp.2397–2402, 1997.

[7] Yue, S. and Henrich, D., *Manipulating Deformable Linear Objects: Sensor-Based Fast Manipulation during Vibration*, Proc. IEEE Int. Conf. Robotics and Automation, pp.2467–2472, 2002.

[8] Terzopoulos, D. *et al.*, *Elastically Deformable Models*, Computer Graphics, Vol. 21, No. 4, pp.205–214, 1987.

[9] Joukhader, A., Deguet, A., and Laugie, C., *A Collision Model for Rigid and Deformable Bodies*, Proc. IEEE Int. Conf. on Robotics and Automation, pp.982–988, Alberquerque, May, 1998.

[10] Galyean, T. A., and Hughes, J. F., *Sculpting: An Interactive Volumetric Modeling Technique*, Computer Graphics, Vol.25, No.4, pp.267–274, 1991.

[11] Rosenblum, R. E., Carlson, W. E., and Tripp, E., *Simulating the Structure and Dynamics of Human Hair: Modelling, Rendering and Animation*, Journal of Visualization and Computer Animation, Vol. 2, No. 4, pp.141–148, 1991.

[12] Belytschko, T., Liu, W. K., and Moran, B., *Nonlinear Finite Elements for Continua and Structures*, John Wiley & Sons, Chapter 9 Beams and Shells, pp.509–568., 2000.

[13] Pai, D. K., *STRANDS: Interactive Simulation of Thin Solids using Cosserat Models*, Computer Graphics Forum. Vol. 21, No. 3, pp.347–352, 2002.

[14] Wakamatsu, H. and Hirai, S., *Static Modeling of Linear Object Deformation Based on Differential Geometry*, Int. J. of Robotics Research, Vol. 23, No. 3, pp.293–311, March, 2004.

[15] Wakamatsu, H., Arai, E., and Hirai, S., *Fishbone Model for Belt Object Deformation*, Burgard, W., Brock, O., and Stachniss, C. eds., *Robotics: Science and Systems III*, The MIT Press, pp.89–96, 2007.